Journal of King Saud University – Computer and Information Sciences xxx (2018) xxx–xxx

Contents lists available at ScienceDirect

Journal of King Saud University – Computer and Information Sciences

journal homepage: www.sciencedirect.com

Holoentropy measures for image stitching of scenes acquired under CAMERA unknown or arbitrary positions

D. Ane Delphin [a,*], Mahabaleswara R. Bhatt [b], D. Thiripurasundari [c]

[a] T. John Institute of Technology, Bangalore, India
[b] BMS College of Engineering, Bangalore, India
[c] VIT University, Chennai, India

ARTICLE INFO

Article history:
Received 10 February 2018
Revised 4 July 2018
Accepted 9 August 2018
Available online xxxx

Keywords:
Image stitching
Panoramic images
Holoentropy
Illumination
Seamless stitching

ABSTRACT

Image stitching of similar scenes is a challenging task when scenes are captured under varying illuminations between the scenes, varying camera positions, varying orientations either in axial or azimuth. In this paper, we explore a seamless image stitching algorithm to address the above-said issues by applying techniques of dehazing on the acquired scenes and before identifying the image features and holoentropy aided feature matching on the Scale Invariant Feature Transform (SIFT) based features for the image. Experimentation of the proposed system is compared with the existing image stitching methods using squared distance, Minkowski and pairwise Euclidean distance for feature matching. The proposed seamless stitching method is evaluated based on the metrics, horizontal square gradient value (HSGV) and vertical square gradient value (VSGV). The obtained results are shown to be feasible for stitching the nonuniform or illumination variation multiple images. The exploration of above said stitching algorithm is intended to reduce the number of computations and inconsistencies in the stitched results.

1. Introduction

The Image stitching technique is used to create a panaramic image from more than one image with overlapped regions that are captured using any digital camera (Huang et al., 2015) or any smartphone camera (Ma et al., 2015). Typically, in biomedical applications, image stitching process arises in microscopic or natural internal organs imaging with a smaller size overlapping images having high resolutions or different resolutions (implied by varying image patches) caused by scale changes to create a single seamless image with high resolution for intended image analysis (Brown and Lowe, 2007) (Candocia, 2003). Also, this image stitching process arises in telescopic imaging systems using satellite or any other airborne camera. Its main objective is to integrate multiple images with overlapped regions to create a seamless and high-resolution image. Image alignment and image blending are very important for generating a high resolution image. The accuracy and efficiency of image stitching are enhanced by the quality of image alignment (Kybic, 2004). Image alignment includes three methods such as transformation domain-based method, intensity-based method (Zitova and Flusser, 2003) and feature-based method (Zoghlami et al., 1997). Among them, a feature-based method is popular for image stitching applications (David and Lowe, 2004). Image stitching consists of three main steps (Zaragoza et al., 2014) – feature matching, homography estimation and seam selection with color blending. Feature matching is based on the correspondence of points. While stitching many images, feature matching would be the time-consuming one.

A large number of image stitching tools are developed including Lowe's method (Yang and Wang, 2013), optimal seam selection algorithm (Boykov and Kolmogorov, 2004), heuristic seam selection algorithm (Mills and Dudek, 2009), Panorama weaving (Summa et al., 2012), Smooth transition algorithms (Peleg, 1981) etc. But these tools have problems because they produce unconvincing results such as yielding misalignment artefacts or ghosting in the results (Zaragoza et al., 2014), time-consuming (Huang et al., 2015) leading to critical bottleneck (Ma et al., 2015), poor stitching performance (Song et al., 2015), blurred image formation (Liu et al., 2008), misalignment (Zhi and Cooperstock, 2012) and stitching noise (Lei et al., 2016).

* Corresponding author.
E-mail address: anedelphin@gmail.com (D. Ane Delphin).
Peer review under responsibility of King Saud University.

Production and hosting by Elsevier

https://doi.org/10.1016/j.jksuci.2018.08.006
1319-1578/

Please cite this article in press as: Ane Delphin, D., et al. Holoentropy measures for image stitching of scenes acquired under CAMERA unknown or arbitrary positions. Journal of King Saud University – Computer and Information Sciences (2018), https://doi.org/10.1016/j.jksuci.2018.08.006

Image stitching using images captured at nonfixed camera positions would encounter the following issues with respect to any two images, namely, (1) Resolution or scale changes due to varying positions between camera and objects while acquiring. (2) Foreshortening or elongation of image formation due to orientation changes between the two acquired images due to either camera or object motions.

The main intention of this proposed novel method is basically to address image stitching using images acquired with arbitrary and unknown camera positions that would result in image stitching challenges having varying scales, rotation and translations.

The main contribution of this paper is Holoentropy aided feature matching: Feature matching based on the holoentropy scheme is introduced in this paper. The key points of the images to be stitched are determined using holoentropy because of the effective representation of nonlinear data and outlier removal characteristics. The noise tolerant behaviour of holoentropy helps to overcome the external influences on images in seamless stitching (Li et al., 2018; Lu et al., 2018; Li et al., 2018; Li et al., 2018). This paper further ensures image stitching under varying illumination environment.

The rest of the paper is organized as follows. Section 2 reviews the related works in image stitching and discusses the problems associated with the state-of-the-art methods. Section 3 details the proposed stitching method with required illustration and mathematical formulations. Section 4 discusses the obtained results and Section 5 concludes the paper.

2. Literature review

2.1. Related research

Though the enormous amount of literature exists, there are only a few attempts that are directed to stitching images pertaining varying illumination scenes. Zaragoza et al. (2014) developed an estimation technique based on Moving Direct Linear Transformation to minimize the problem of ghosting without any changes in the image stitching views. Here, Singular Value Decomposition (SVD) method has been used to determine the closest points for stitching. The SVD measurements suffer practical challenges such as outliers, illumination variation and noise. Hence, secondary methods are required to handle such issues. Also, this technique is computation inefficient due to SVD.

Ma et al. (2015) have exploited RANSAC and Weighted average bending algorithm for finding the optimum affine-transformations and smoothening the intensities of the overlapping regions, respectively. However, the hamming distance based similarity measure adopted here explores minor deviations from its original intensity and hence it fails to determine the precise similarity between the images under varying illumination. Huang et al. (2015) have determined the stitching similarities using maximum likelihood estimation process. Despite being able to handle nonlinear image intensities, the likelihood estimation process is sensitive to initialization and number of samples. The context of chaos theory has been adopted in Song et al. (2015) for determining the similarity between the images. The chaos theory is a renowned intelligent methodology, yet the complexity of the representation of the image increases the computing complexity. The greedy search adopted in Li et al. (2015) is a local search algorithm and hence the probability of sticking with the local minima is high.

Lei et al. (2016) developed a 3D image stitching method which is based on noise mechanism analysis. Here, correlation analysis has been deployed to understand the dissimilarity among the stitching images. However, the correlation analysis is prone to chaotic noise and so misalignment often happens in the stitching process.

In 2009, Morel and Guoshen (2009) proposed Affine-SIFT (ASIFT) image matching algorithm extends the SIFT method to a fully affine invariant device. It has attempted to prove that mathematical arguments by a new algorithm that a fully affine invariant image matching is possible.

In 2010, Rosten et al. (2010) presented the FAST family of detectors. In addition, they turned the simple and repeatable segment test heuristic into the FAST-9 detector that has unmatched processing speed by machine learning. In spite of the design for speed, the resulting detector has excellent repeatability.

In 2012, Alahi et al. (2012) proposed a novel keypoint descriptor, which inspired by the human visual system and more accurately the retina, termed Fast Retina Keypoint (FREAK). A cascade of binary strings is calculated by efficiently comparing image intensities over a retinal sampling pattern.

Table 1 comprehensively gives review outcome of the state-of-the-art similarity measurement methodologies for image stitching process and the critics on them in the lines of adopted methodology. Close observing the current literature, there is less information on the consideration of external constraints such as varying illumination, outliers and noise, especially in image stitching involving images captured with low light imaging camera systems.

2.2. Image stitching for overlapped images but captured at nonfixed camera positions

In this paper, we explore an image stitching process to create a wide angle or wide area or panaorama image using multiple overlapped images acquired using either handheld or smartphone camera, which is not assured to be in a fixed position would suffer from the following two kinds of image parameters issues:

1) Geometric image transformation feature parmeters such as rotation, scale (resolution), translate positions may differ from other images (consider overlapped region) would suffer from unknown values that are dependent on camera position, which may not hold fixed while imaging.
2) Photometric image transformation features such as brightness, contrast, sharpness and saturation, may differ in each image dependent on the source of illumination, exposure, view angle variation, scattering and absorption of media and object whose image are to be captured would result in varying illumination effect. Further, while imaging of any live wet tissue of the organ in biomedical field yields images with varying contrast due to the scattering and absorption of light or a non-uniform illuminated images.

Table 1
State-of-the-art similarity measures adopted in image stitching process.

Author [Citation]	Adopted Methodology	Drawbacks
Lei et al. (2016)	Correlation	Chaotic noise
Ma et al. (2015)	Hamming distance	Susceptible to Illumination variant
Huang et al. (2015)	Maximum likelihood	Sensitive to initial values and low dimensional data
Zaragoza et al. (2014)	Singular value decomposition	Prone to outlier and huge computational complexity
Song et al. (2015)	Chaos theory	Huge computational complexity
Li et al. (2015)	Greedy search algorithm	Local searching characteristics

Please cite this article in press as: Ane Delphin, D., et al. Holoentropy measures for image stitching of scenes acquired under CAMERA unknown or arbitrary positions. Journal of King Saud University – Computer and Information Sciences (2018), https://doi.org/10.1016/j.jksuci.2018.08.006

3. Image stitching based on holoentropy aided SIFT feature matching

In this section, a detailed discussion about the proposed methodology is deliberated. The overall block diagram of the proposed methodology is shown in Fig. 1. Initially, the images with overlap areas are accepted as the input for the stitching procedure. Because the noise is inevitable especially sensor noise during a low light condition of image acquisition, the preprocessing noise removal is adopted.

In contrast to any conventional image stitching methods, the proposed image stitching method helps noise removal so that the practical viabilities of the proposed method are increased. The features of the images are vital for accurate stitching of the images. Here, feature extraction is accomplished using SIFT, because SIFT features are known to be invariant to a scene change, rotation, blurring etc. in the image. The extracted features from the images are subjected to feature matching process. The features in the overlapped images are matched using cost function enabled by holoentropy based upon the estimated maximum holoentropy value. Image matching follows feature matching.

The objective of image matching is to find the matching points of the images based on maximum feature match. Using RANSAC, the inliers between the images with compatible homography are selected. In image matching, errors due to the concatenation of the pairwise homographies are adjusted using the bundle adjuster. In bundle adjustment, the sum of the squared image distance (sum of the squared distance of two images to be stitched) is minimized regarding the images parameter. Lastly, blending of images is done. Image blending results in a panoramic image of the overlapped images accepted as the input.

3.1. SIFT feature extraction

The major steps involved in SIFT feature extraction (Brown and Lowe, 2007) procedure are; (i) Scale Space Extrema detection (ii) Key point localization (iii) Orientation Assignment and (iv) Key point descriptor (David and Lowe, 2004). The key locations representing the SIFT features are defined as the maxima and minima result of the difference of Gaussian function applied in scale space to the input images. The steps evolved to ensure that the key points are more stable for the feature matching leading to image matching.

1. Detection of Scale-Space Extrema: The point of interest is nothing but the Key points. It is effectively achieved by making use of Gaussian difference function (DOG), since the images are convolved with Gaussian filters at different scales. The DOG function increases the visibility of the edges in the images. For the input image I with $M \times N$ number of the pixels, the scale space function is defined as

$$L_{m,n}(\sigma) = G_{m,n}(\sigma) * I_{m,n} \tag{1}$$

where, $m = 1, 2, \ldots, M$, $n = 1, 2, \ldots, N$, $*$ is the convolution function, *isthevariablescaleGaussianfunction*, is the variable scale Gaussian function, σ is the scale value and $I_{m,n}$ is the input image. The difference of Gaussian (DOG) is used to detect the stable key point as given in (2) below:

$$D_{m,n}(\sigma) = L_{m,n}(K_s\sigma) - L_{m,n}(K_t\sigma) \tag{2}$$

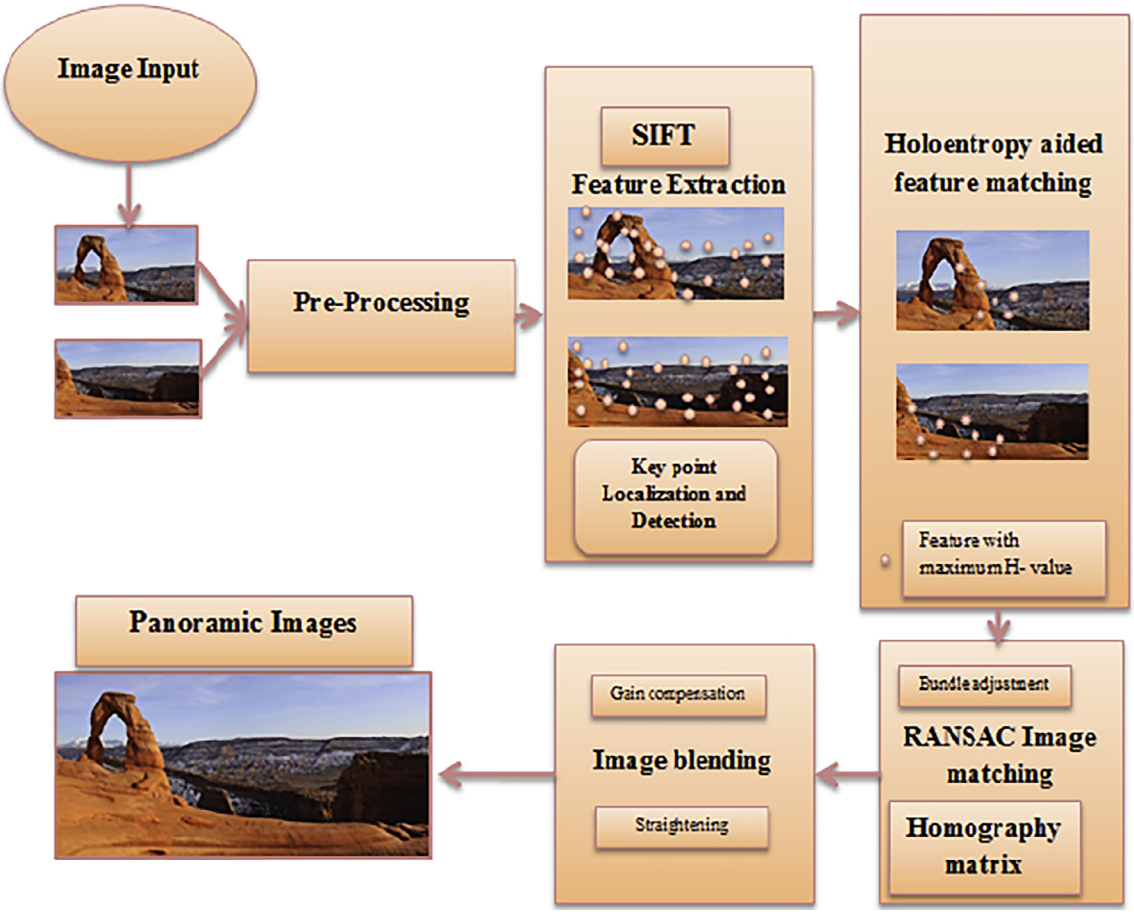

Fig. 1. Architecture of Image stitching based on Holoentropy aided SIFT feature matching.

Please cite this article in press as: Ane Delphin, D., et al. Holoentropy measures for image stitching of scenes acquired under CAMERA unknown or arbitrary positions. Journal of King Saud University – Computer and Information Sciences (2018), https://doi.org/10.1016/j.jksuci.2018.08.006

where, $K_s\sigma$ and $K_t\sigma$ specifies the variation in the scale values. The scale space feature using DOG can be computed using simple subtraction. In order to find the local minima and maxima of DOG, the key point is compared with the neighbors in the image.

2. Precise Key Point localization: Scale-space extrema detection generates more number of key points. In key point localization, the key points are selected based on the measure of their stability (David and Lowe, 2004; Yang and Guo, 2008).

a) To eliminate key points associated with contrast:. Interpolation is done using the Taylor series expansion of DOG as given in Eq. (3), where, D is estimated at the candidate key point with $C_{m,n}(\sigma)$ as the offset (Li et al., 2008).

$$D(T) = D + \frac{\partial D^T}{\partial T}T + \frac{1}{2}T^T\frac{\partial^2 D^T}{\partial T^2}T \tag{3}$$

b) To eliminate key points associated with the edge responses: DOG function may choose the key points in the location with high edge response (Yang and Guo, 2008). In order to overcome this effect, the key points are selected based on stability. By finding the principle curvature of the peaks in DOG function, the edgy responses can be neglected. Since the edgy responses have higher principal curvature values, it is easier to eliminate. On noting the equivalence between principal curvature and Eigenvalues of the second order Hessian Matrix, H_m that is obtained from (3) represented as:

$$H_m = \begin{bmatrix} D_{mm} & D_{mn} \\ D_{nm} & D_{nn} \end{bmatrix} \tag{4}$$

the key points associated with the edgy responses are excluded based on the absolute difference value.

3. A consignment of Orientation to key points: In this step, the local image gradient direction induced orientations are assigned to the key points. Hence, the invariance to image rotation can be achieved by the SIFT features (David and Lowe, 2004; Li et al., 2008). Given a Gaussian smoothed function $L_{m,n}(\sigma)$, the gradient magnitude g and the orientation θ (Fang et al., 2010) f the key point are determined using Eqs. (5) and (6).

$$g_{m,n} = \sqrt{\left[(L_{m+1,n} - L_{m-1,n})^2 + (L_{m,n+1} - L_{m,n-1})^2\right]} \tag{5}$$

$$\theta_{m,n} = \tan^{-1}[(L_{m,n+1} - L_{m,n-1}), (L_{m+1,n} - L_{m-1,n})] \tag{6}$$

4. Key point descriptor vector: In the key point descriptor (Brown et al., 2005), from the gradient magnitude and orientation values of the key point, histograms are computed. Each histogram contains the values from the neighborhood of the considered key points. The values of the histograms are converted into a descriptor vector by adding a weighted Gaussian function to the gradient magnitude with scale equal to the length of the descriptor window. Normalization of the descriptor vector achieves the invariance in the affine

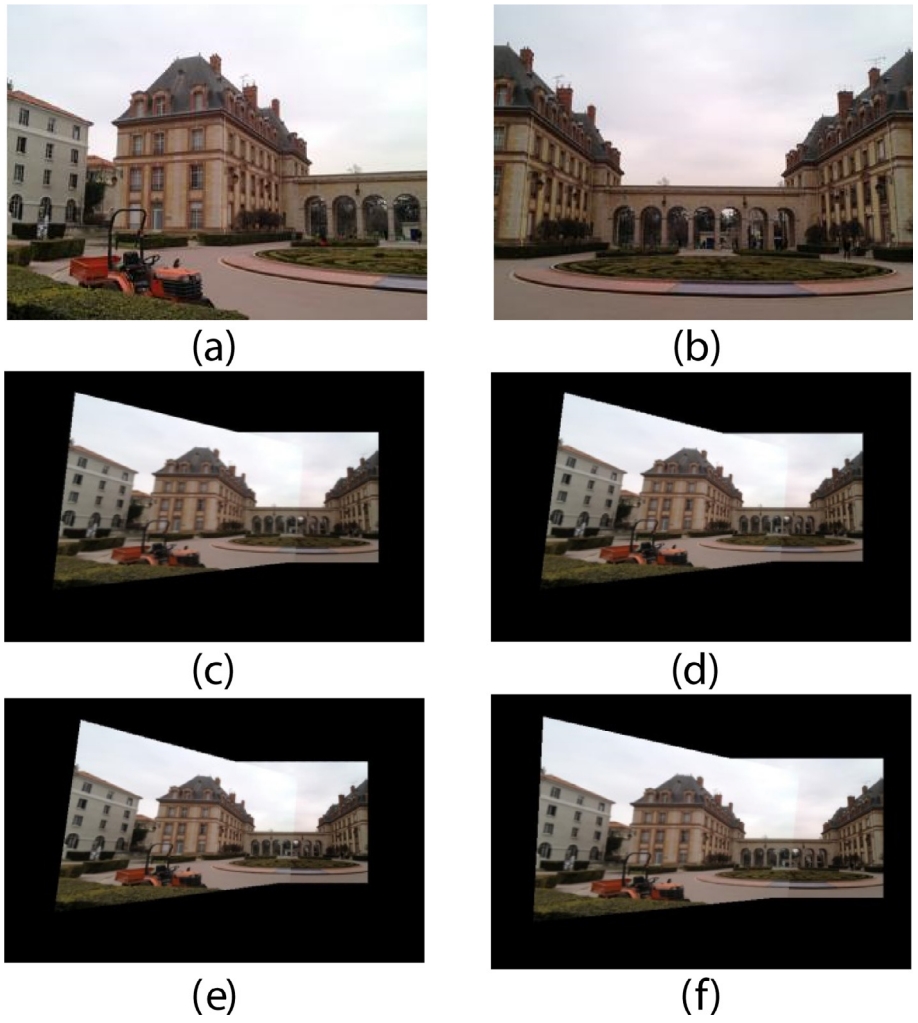

Fig. 2. Results under normal conditions, (a) and (b) Images at different points, Stitched image from methods based on (c) Euclidean distance, (d) Minkowski distance, (e) pairwise Euclidean distance and (f) Holoentropy based matching.

Please cite this article in press as: Ane Delphin, D., et al. Holoentropy measures for image stitching of scenes acquired under CAMERA unknown or arbitrary positions. Journal of King Saud University – Computer and Information Sciences (2018), https://doi.org/10.1016/j.jksuci.2018.08.006

Table 2
Stitching performance of various methods under normal conditions.

HSGV					
Similarity Measures	Image 1	Image 2	Image 3	Mean	Rank
Euclidean	345.71	72.276	290.23	236.072	4
Minkowski	799.51	70.19	292.6	387.4333	3
Pairwise Euclidean	813.99	77.767	276.52	389.4257	2
ASIFT (Morel and Guoshen, 2009)	339.72	89.07	346.98	267.90	7
FAST (Rosten et al., 2010)	323.80	96.56	378.09	256.32	6
FREAK (Alahi et al., 2012)	314.09	92.76	365.04	357.98	5
Chaos-inspired (Song et al., 2015)	298.98	102.43	468.12	333.43	8
Holoentropy	359.01	186.15	725.83	423.6633	1
VSGV					
Similarity Measures	Image 1	Image 2	Image 3	Mean	Rank
Euclidean	739.21	241.88	592.94	524.6767	4
Minkowski	744.25	248.67	594.07	528.9967	3
Pairwise Euclidean	784.24	273.31	615.58	557.71	1
ASIFT (Morel and Guoshen, 2009)	645.89	214.78	456.87	342.23	5
FAST (Rosten et al., 2010)	677.93	209.67	498.90	358.87	7
FREAK (Alahi et al., 2012)	623.66	198.76	367.04	478.90	8
Chaos-inspired (Song et al., 2015)	611. 97	188.45	379.39	524.78	6
Holoentropy	751.59	220.49	694.73	555.6033	2

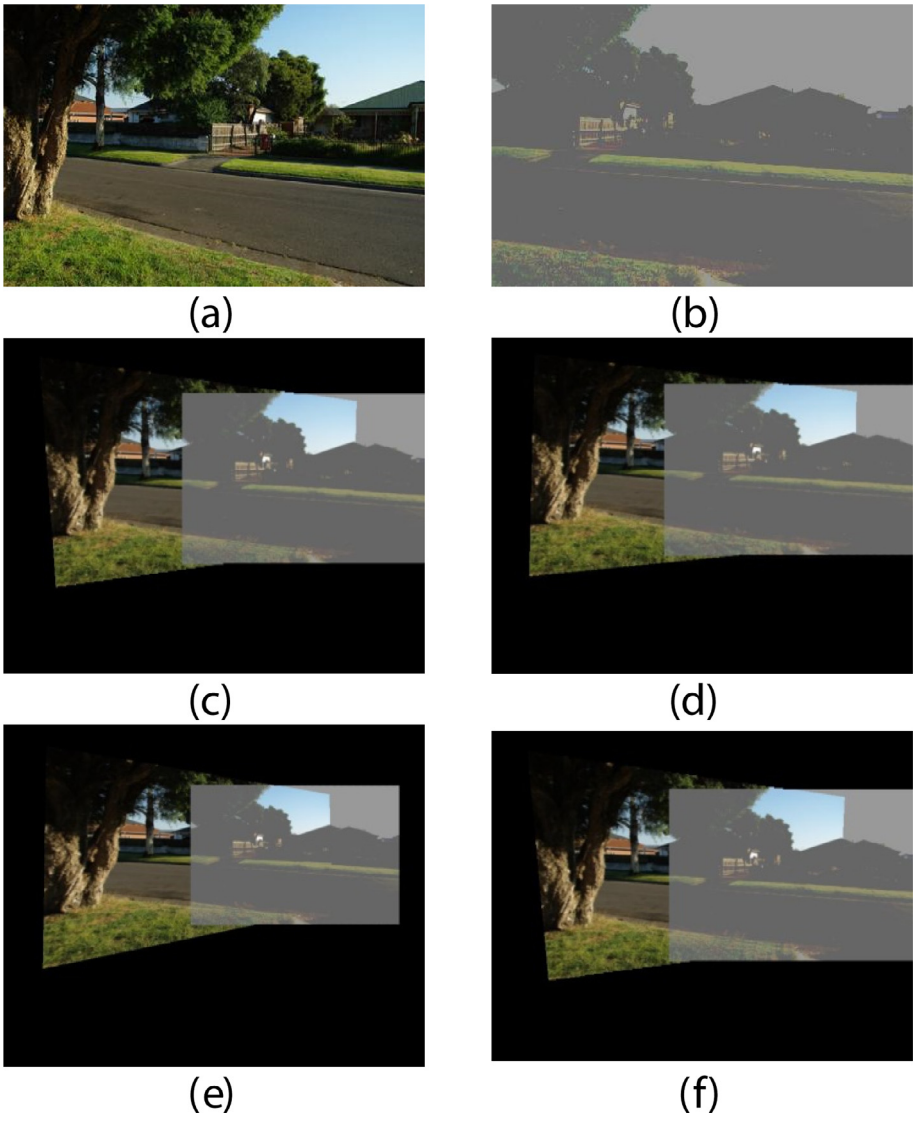

Fig. 3. Results under varying illumination, (a) Image without any effect of illumination and (b) Image with illumination. Stitched image from methods based on (c) Euclidean distance, (d) Minkowski distance, (e) pairwise Euclidean distance and (f) Holoentropy based matching.

Please cite this article in press as: Ane Delphin, D., et al. Holoentropy measures for image stitching of scenes acquired under CAMERA unknown or arbitrary positions. Journal of King Saud University – Computer and Information Sciences (2018), https://doi.org/10.1016/j.jksuci.2018.08.006

changes and non-linear illumination effect is reduced by applying a threshold value to the vector followed by normalization (David and Lowe, 2004). The feature vector extracted using SIFT for the input images I_1 and I_2 can be represented as *and* and $B = [a_{i,n}] \in R^{m_2 \times N}$, respectively, where, $i = 1, 2, \ldots, m_1, j = 1, 2, \ldots, m_2$, and n = 1,2,$\cdots N$.

3.2. Holoentropy enabled feature matching

Commonly, some metrics mentioned in Ma et al., (2015), Hua and Li (2010) or likelihood information is used to extract and match the relevant image features (Lei et al., 2016; Huang et al., 2015). But, the matching is to be performed between the features of two images having some overlapping portions and the same need to be continued across multiple images one after the other. Especially, while feature matching between any corresponding to overlapped regions that involves more than one image requires either to perform maximization of correlation for best matches by similarity or reduction of dissimilar wrong matches by minimizing entropy, simultaneously. Interestingly, both of them are complementary to each other. Our motivation factors are to reduce the dissimilar matches that are not belonging to the overlapped regions, at the same time maximize similarity features belonging to the overlapped region, which are having geometric and photometric variations in the overlapped regions of the images.

In order to combine both the above-stated characteristics we recall the holoentropy formulated by Watanabe (Ganesa Moorthy and Nandhini Devi, 2014) and exploit this as holoentropy enabled feature matching. The Holoentropy utilized for Image matching includes determining the holoentropy of the features associated with the images and selecting the feature vector element, which has maximum holoentropy values as the best feature in the images. Subsequently, image stitching is done using the extracted features. Holoentropy is the summation of both the entropy and the total correlation (Shu and Wang, 2013). The steps involved in the holoentropy enabled feature matching are given below.

Essentially, the features with maximum H value are selected as the optimal feature among the feature vectors of the input image. In other words, the Holoentropy is a transformation of feature vector of the image. It provides precise information statistics of the feature vector. Instead of finding the similarity between the feature vectors, the proposed process finds the similarity between the feature vectors, which have increased holoentropy, which are called as optimal feature vector. This provides more precise similarity among the images points.

Further, entropy is generally used as a measure to detect the unmatched features (Shu and Wang, 2013). For the entropy value calculated over the feature vector, if the value of entropy decreases when a feature is neglected, it specifies that feature to be unmatched. In information theory, the entropy value aids in the prediction of the correct value, even if the value of the attribute is unknown. Entropy is calculated based on the chain rule, which can be simplified as given in (7) below:

$$E_{ij} = -P_{ij} \log P_{ij} \tag{7}$$

where, the value of *in* in (7) is regarded as a ratio dependent on both correlation and total correlation due to the individual features are given as (10).

$$P_{ij} = \frac{|C_{ij}|}{TC_r} \tag{8}$$

Now, on noting the correlation between the standard feature vectors of the images I_1 and I_2 as

Table 3
Stitching performance of various methods under varying illumination effect.

HSGV						
Similarity measures	Illumination effect	Image 1	Image 2	Image 3	Mean	Rank
Euclidean	1	587.58	128.48	478.46	478.46	3
	2	611.56	416.23	464.53	464.53	4
Minkowski	1	558.43	281.71	799.08	799.08	1
	2	580.75	423.42	468.82	468.82	3
Pairwise Euclidean	1	532.43	386.3	497.1	497.1	2
	2	464.17	236.68	516	516	2
ASIFT (Morel and Guoshen, 2009)	1	578.33	242.71	722.18	789.18	2
	2	590.75	483.52	454.22	438.12	4
FAST (Rosten et al., 2010)	1	527.27	138.48	412.46	423.36	2
	2	621.36	414.23	434.53	434.33	3
FREAK (Alahi et al., 2012)	1	533.44	323.3	437.1	426.1	2
	2	413.15	224.68	545.23	528.4	4
Chaos-inspired (Song et al., 2015)	1	537.28	164.48	448.36	428.46	3
	2	631.36	416.23	424.33	444.33	3
Holoentropy	1	1110.6	131.29	356.46	356.46	4
	2	678.98	218.06	969.88	969.88	1
VSGV						
Similarity measures	Illumination effect	Image 1	Image 2	Image 3	Mean	Rank
Euclidean	1	1051.7	321.51	947.18	773.4633	1
	2	1027.4	361.96	922.49	770.6167	3
Minkowski	1	1018.7	294.04	885.14	732.6267	3
	2	1025.3	374.82	935.28	778.4667	2
Pairwise Euclidean	1	965.78	372.11	977	771.63	2
	2	504.32	355.09	1155.1	671.5033	4
ASIFT (Morel and Guoshen, 2009)	1	1011.8	341.21	923.28	763.42	3
	2	1037.6	331.93	932.47	761.64	1
FAST (Rosten et al., 2010)	1	1128.6	263.16	845.24	712.63	2
	2	1135.2	326.84	934.18	722. 7	3
FREAK (Alahi et al., 2012)	1	923.73	333.12	934.2	732. 33	3
	2	504.34	344.19	1235.1	643.53	2
Chaos-inspired (Song et al., 2015)	1	1052.76	324.31	923.18	722. 33	1
	2	1023.6	361.46	924.59	799.62	4
Holoentropy	1	984.94	328.83	785.82	699.8633	4
	2	1175.2	378.16	962.31	838.5567	1

Please cite this article in press as: Ane Delphin, D., et al. Holoentropy measures for image stitching of scenes acquired under CAMERA unknown or arbitrary positions. Journal of King Saud University – Computer and Information Sciences (2018), https://doi.org/10.1016/j.jksuci.2018.08.006

$$C_{ij} = 1 - \frac{1}{2N} d_{ij}^2 \tag{9}$$

and total correlation as the sum of possible correlations

$$TC_r = \sum_{i=1}^{m_1} \sum_{j=1}^{m_2} [C_{ij}] \tag{10}$$

where the Euclidean distance *on* on

using the feature sets defined as $A = [a_{i,n}] \in \mathrm{R}^{m_1 \times N}$ and $B = [a_{i,n}] \in R^{m_2 \times N}$, respectively, where, $i = 1, 2, \ldots, m_1$, $j = 1, 2, \ldots, m_2$, and *as* as

Optimizing the total correlation and joint entropy are independent objectives, where total correlation needs to be maximized and joint entropy needs to be minimized.

Holoentropy treats all the attributes with equal importance. However, the real data set has different weightage. In order to weigh the entropy relied on each attribute, reverse sigmoid function (Shu and Wang, 2013) is used. Hence, holoentropy, H is represented as (11),

$$H = w_{ij} + H_{ij} \tag{11}$$

where, the value of H_{ij} is the combination of the entropy value

$$H_{ij} = E_{ij} + C_{ij} \tag{12}$$

and w_{ij} as:

$$w_{ij} = \frac{2}{1 + e^{(-H_{ij})}} \tag{13}$$

Note also H_{ij} denotes holoentropy value without weighted reverse sigmoid function.

3.3. Image matching and blending

In image matching, the images with maximum feature matches are collected. The collected images are finally stitched into a panoramic image. Since each image taken for reconstruction overlaps with the other, the features may match with every possible image. Hence, it is necessary to match the image with a small number of overlapping images so that good solution for image geometry can be chosen. RANSAC (Li et al., 2008) solves the purpose by selecting the image with feature matches compatible to homography between the images. The feature point with a correct match to the input image (reference image) is called inlier and the feature point without a correct match is called an outlier. RANSAC intends to acquire a significant set of data points with the inliers by the rejection of outliers which is achieved by a set of model parameters (Yang and Guo, 2008). The model parameter set with higher support is considered to be the correct/compatible homography. The inliers generated by RANSAC are verified using probabilistic model. The probabilistic model (Li et al., 2008) compares the probabilities of inliers or outliers generated by correct or false match. By the application of RANSAC, image matches between the two images are attained. The problem here is to eliminate the accumulated error between the images. By using bundle adjuster (Brown and Lowe, 2007), the error is minimized. In bundle adjustment, parameters of the homography matrix are optimized constantly, until the residual error due to the accumulation of the image is decreased.

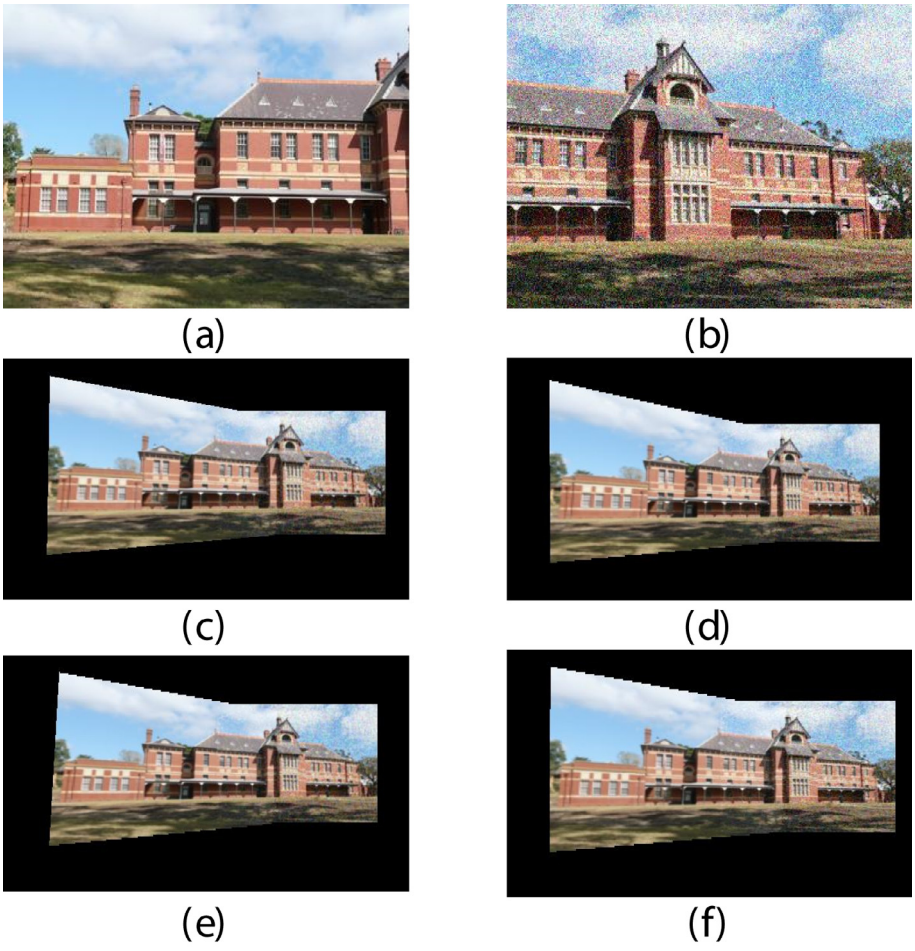

Fig. 4. Stitching results under noisy environment. Images to be stitched (a) noise-free image and (b) noisy image. Stitched image from methods based on (c) Euclidean distance, (d) Minkowski distance, (e) pairwise Euclidean distance and (f) Holoentropy based matching.

Please cite this article in press as: Ane Delphin, D., et al. Holoentropy measures for image stitching of scenes acquired under CAMERA unknown or arbitrary positions. Journal of King Saud University – Computer and Information Sciences (2018), https://doi.org/10.1016/j.jksuci.2018.08.006

Image blending is the fusion/integration of the images (based on the matched images). Image matching using RANSAC method results in image stitching geometry, with the seam in the overlap region (Li et al., 2008). The objective of image blending is to stitch the images to spawn panoramic images seamlessly. For the precise reconstruction of the images with overlap, blur, etc. into panoramic images, some of the techniques in addition to fusion are endured. They are 1) Straightening 2) Gain Compensation 3) Multi-band blending (Brown and Lowe, 2007). Straightening is a method by which wavy effect from the output panoramas is removed effectively. Gain compensation is the technique adapted in image fusion to nullify the intensity error for all the overlapping pixels. The edges in the images which are visible even after gain compensation, parallax effect, misregistration errors etc. are reduced by multi-band blending strategy.

4. Results and discussion

4.1. Procedure

The experimentation is carried out in a computing machine with Intel Core i3 Processor, 2 GB RAM and Windows operating system. The simulation is done using the MATLAB R2014a. The experimental procedure is as follows. Initially, two images with overlap region without having any noise or the illumination effect is given as the input for the image stitching scheme. The proposed scheme results in the quality panoramic image with less time for computation. Secondly, an image with illumination effect is given as the input and stitched into panoramic image without any variation in the stitching performance because of the illumination effect. Lastly, an image with the noisy environment is given as the input. In experimentation, five noise variation images are used for the stitching purpose. The resulted panoramic image is invariant to the noise effect. Two performance metrics namely, "Horizontal Square Gradient Values" and "Vertical Square Gradient Values" (Song et al., 2015), which are given in Eqs. (14) and (15) respectively, are used to evaluate the stitching performance on the stitched image.

$$HSGV = \sum_{m=1}^{M}\sum_{n=1}^{N}\left|\widehat{I}\,(m,n+1) - \widehat{I}\,(m,n)\right|^2 \tag{14}$$

$$VSGV = \sum_{m=1}^{M}\sum_{n=1}^{N}\left|\widehat{I}\,(m+1,n) - \widehat{I}\,(m,n)\right|^2 \tag{15}$$

The performance of the proposed stitching system is compared with the existing methods like squared distance (Brown and Lowe, 2007) and its variants, Minkowski and pairwise Euclidean distance. The obtained results on the image stitching under normal conditions, images with the noise and images with illumination effects are discussed here.

4.2. Under normal conditions

Fig. 2 shows the stitching performance of multiple methods under normal conditions. Fig. 2(a) and (b) are the images acquired from different points and Fig (c–f) refers to the panoramic images obtained from all the methods.

Table 4
Stitching performance in terms of HSGV of stitched images resulted from various methods under noisy environment.

Feature Matching	Noise variation	Image 1	Image 2	Image 3	Mean	Rank
Euclidean	0.005	494.51	142.84	577.77	405.04	4
	0.01	296	203.38	912.95	470.7767	4
	0.015	425.42	295.25	681.15	467.2733	4
	0.02	882.14	220.31	1283.2	795.2167	1
	0.025	859.02	283.72	885.99	676.2433	1
Minkowski	0.005	815.66	136.34	599.57	517.19	2
	0.01	438.18	148.77	902.27	496.4067	1
	0.015	969.75	206.65	862.46	679.62	2
	0.02	618.66	381.85	1160	720.17	2
	0.025	449.36	264.17	883.57	532.3667	2
Pairwise Euclidean	0.005	389.2	198.09	1054.3	547.1967	1
	0.01	339.08	214.12	865.55	472.9167	3
	0.015	1035.5	226.6	799.3	687.1333	1
	0.02	1061.6	278.73	764.93	701.7533	3
	0.025	434.43	3.6127	39.134	159.0589	4
ASIFT (Morel and Guoshen, 2009)	0.005	321.45	123.54	543.34	328.65	3
	0.01	326.78	132.45	708.86	367.21	2
	0.015	621.34	165.43	654.32	532.12	1
	0.02	503.43	254.23	934.54	543.23	4
	0.025	421.65	431.76	229.54	324.54	4
FAST (Rosten et al., 2010)	0.005	284.34	129.65	543.67	324.65	2
	0.01	331.23	124.56	745.54	523.43	3
	0.015	623.49	170.98	734.65	532.45	4
	0.02	505.67	257.89	957.86	547.80	4
	0.025	431.67	439.54	229.65	378.45	1
FREAK (Alahi et al., 2012)	0.005	356.78	124.87	645.67	321.78	2
	0.01	345.89	132.39	762.45	390.09	3
	0.015	641.34	173.23	699.02	537.72	4
	0.02	505.56	254.76	976.40	548.50	2
	0.025	423.56	412.98	231.42	331.45	2
Chaos-inspired (Song et al., 2015)	0.005	345.67	129.76	675.89	325.69	4
	0.01	342.78	134.67	765.54	398.7	3
	0.015	675.43	178.16	765.32	543.17	1
	0.02	514.67	276.43	989.76	569.98	2
	0.025	434.36	435.78	234.65	345.23	3
Holoentropy	0.005	387.53	134.12	712.64	411.43	3
	0.01	365.42	171.88	898.91	478.7367	2
	0.015	757.76	207.52	803.48	589.5867	3
	0.02	529.44	290.82	1002.1	607.4533	4
	0.025	440.57	471.42	259.99	390.66	3

Please cite this article in press as: Ane Delphin, D., et al. Holoentropy measures for image stitching of scenes acquired under CAMERA unknown or arbitrary positions. Journal of King Saud University – Computer and Information Sciences (2018), https://doi.org/10.1016/j.jksuci.2018.08.006

Table 5
Stitching performance of various methods under noisy environment.

Feature Matching	Noise variation	Image 1	Image 2	Image 3	Mean	Rank
Euclidean	0.005	451.16	326.41	892.59	556.72	4
	0.01	307.45	401.84	1204.8	638.03	4
	0.015	487.8	330.99	1073.1	630.63	4
	0.02	1008.1	431.12	1701.6	1046.94	2
	0.025	765.26	517.88	869.33	717.49	3
Minkowski	0.005	791.08	314.61	975.49	693.7267	3
	0.01	789.52	315.18	1194.4	766.3667	2
	0.015	993.11	338.83	1122.3	818.08	3
	0.02	1084.5	527.63	1544.5	1052.21	1
	0.025	766.56	379.04	852.84	666.1467	4
Pairwise Euclidean	0.005	763.46	336.3	1074.3	724.6867	2
	0.01	722.99	391.46	1172.6	762.35	3
	0.015	980.71	411.84	1194.7	862.4167	2
	0.02	1096.6	472.66	767.06	778.7733	4
	0.025	447.12	7.5926	101.57	185.4275	2
ASIFT (Morel and Guoshen, 2009)	0.005	675.29	298.89	989.76	654.89	3
	0.01	714.78	304.76	1006.45	455.97	3
	0.015	897.87	234.56	1234.76	768.90	1
	0.02	1109.7	376.89	876.98	789.56	2
	0.025	897.09	456.78	265.90	456.90	4
FAST (Rosten et al., 2010)	0.005	567.89	198.78	879.09	568.94	4
	0.01	678.90	289.76	998.78	389.76	3
	0.015	678.98	289.67	967.89	678.90	4
	0.02	987.90	278.54	765.87	654.89	1
	0.025	845.67	387.90	256.86	433.21	2
FREAK (Alahi et al., 2012)	0.005	678.45	281.23	1106.7	717.89	2
	0.01	698.67	303.56	988.56	756.89	3
	0.015	1120.8	324.67	967.89	924.76	4
	0.02	897.65	456.87	876.56	789.65	1
	0.025	902.34	534.76	197.65	489.67	3
Chaos-inspired (Song et al., 2015)	0.005	654.45	276.78	1109.5	698.76	4
	0.01	689.56	312.34	1198.5	675.78	4
	0.015	956.78	289.67	1024.76	789.67	1
	0.02	1034.7	367.98	845.67	786.34	2
	0.025	897.56	489.34	254.78	463.76	3
Holoentropy	0.005	759.14	303.87	1119.1	727.37	1
	0.01	755.71	317.28	1248.7	773.8967	1
	0.015	1131.3	346.25	1336.6	938.05	1
	0.02	1115.6	497.57	979.74	864.3033	3
	0.025	914.5	540.86	275.38	576.9133	1

The comparative evaluation specifying the HSGV and VSGV values of the proposed and conventional stitching methods such as Euclidean, Minkowski, Pairwise Euclidean, ASIFT (Morel and Guoshen, 2009), FAST (Rosten et al., 2010), FREAK (Alahi et al., 2012) and Chaos-inspired (Song et al., 2015) is shown in Table 2. The proposed method attained the maximum HSGV value of 423.6633 which is 8% higher than pairwise Euclidean distance based stitching, and 8.5% higher than Minkowski distance based stitching. The worst case performance of HSGV value, i.e., 236.072 is achieved by the renowned Euclidean distance based image stitching. The VSGV value of Minkowski distance based stitching reached the limit of 528.6767, which is 5.2% lesser than the maximum value, 555.6033 attained by proposed stitching. Euclidean distance based image stitching again attains the worst case scenario of VSGV. Hence, the proposed stitching secures the first rank among all the four methods that illustrate the quality maintained in the stitched images.

4.3. Under illumination variation

The panoramic image resulted in the input acceptance as the image with the illumination effect is shown in Fig. 3. In the course of experimentation, two illumination effects are added along with the normal image for evaluating the seamless stitching performance without any effect of the illumination variation. In order to perform such investigation, one of the two images to be stitched is subjected to high illumination condition, i.e., the white effect has been added more. The resultant stitched images from the four stitching methods are given in Fig. 3.

In Table 3, the stitching performance of the various methods under varying illumination effects 1 and 2 are shown in terms of both HSGV and VSGV. Under illumination effect 1, the worst case HSGV value of 356.46 is attained by the proposed method. Minkowski distance based stitching achieves the maximum value of 799.08. However, in the image stitching with the illumination effect 2, based on the rank value estimated, it is clear that the proposed method provides feasible stitching with increased HSGV value. The maximum value attained by the proposed method with illumination effect 2 is of 4.68% higher than pairwise Euclidean distance based stitching, 5.17% higher than Minkowski distance based stitching and 5.21 higher than Euclidean distance based stitching, which is the vilest case.

The VSGV value managed by the proposed method is lesser than the other methods under illumination effect 1. Under illumination effect 2, the best VSGV value of 838.5567 is reached by the proposed method which is 19.92% greater than the VSGV value of pairwise Euclidean distance based stitching, 7.1% greater than Minkowski distance based stitching and 8.1% greater than VSGV value reached by Euclidean distance based stitching. The increased HSGV and VSGV value obtained at the end of the proposed system for the image with the varying illumination effects proves the efficiency of the stitching invariant to the effect of the illumination and also perseverance of the sharpness perspective.

Please cite this article in press as: Ane Delphin, D., et al. Holoentropy measures for image stitching of scenes acquired under CAMERA unknown or arbitrary positions. Journal of King Saud University – Computer and Information Sciences (2018), https://doi.org/10.1016/j.jksuci.2018.08.006

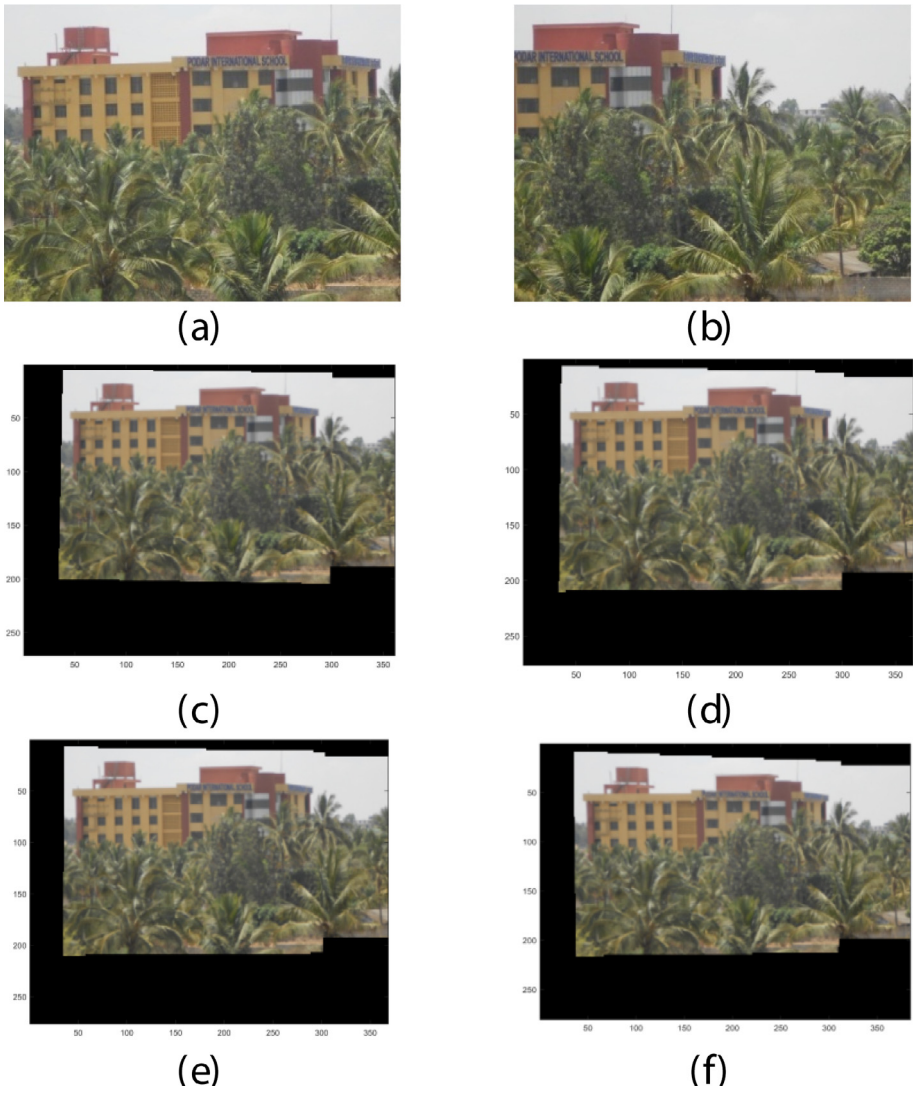

Fig. 5. (a) and (b) Images captured at different camera positions, (c) Stitched image from methods based on (c) Euclidean distance, (d) Minkowski distance (e) pairwise Euclidean distance and (f) Holoentropy based matching.

Table 6
Stitching performance of various methods.

Similarity Measures	HSGV	Rank	VSGV	Rank
Euclidean	163.74	3	399.35	2
Minkowski	162.98	4	394.26	3
Pairwise Euclidean	179.91	2	394.25	4
ASIFT (Morel and Guoshen, 2009)	154.23	5	392.32	5
FAST (Rosten et al., 2010)	145.03	6	388.23	6
FREAK (Alahi et al., 2012)	133.45	7	386.22	7
Chaos-inspired (Song et al., 2015)	123.63	8	384.23	8
Holoentropy	480.38	1	407.15	1

4.4. Under noisy environment

Fig. 4 shows the stitched panoramic image from noisy images. The experimentation is carried out by contaminating one of the images to be stitched by Gaussian noise with its ratio under image as 0.005, 0.01, 0.015, 0.02and 0.025. The stitching performance under such five noise variations is observed in terms of HSGV and VSGV and tabulated in IV and V, respectively.

In Table 4, when stitching is performed between the normal image and the image with the noise level of about 0.005, the best HSGV value 547.1967 is obtained by stitching that uses Minkowski distance as feature matching entity. At the noise variation 0.005, the HSGV value of the proposed method is lower than Minkowski distance based stitching but greater than the values achieved by Euclidean distance based stitching. Under 0.01noise variant, the proposed method has attained the HSGV value of 478.7367, which is 1.66% greater than the HSGV value of Euclidean distance based stitching which is the vilest case among the existing methods taken into consideration for the experimentation. According to Table 5, the proposed stitching has reached the maximum of VSGV

Please cite this article in press as: Ane Delphin, D., et al. Holoentropy measures for image stitching of scenes acquired under CAMERA unknown or arbitrary positions. Journal of King Saud University – Computer and Information Sciences (2018), https://doi.org/10.1016/j.jksuci.2018.08.006

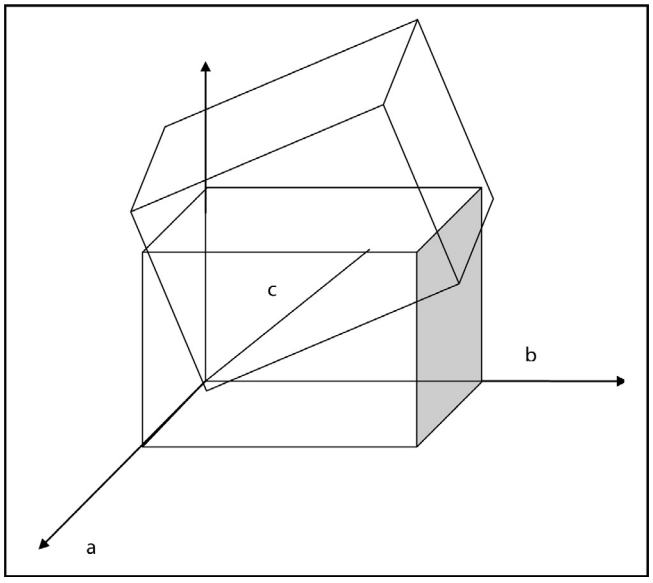

Fig. 6. Camera position at different angles.

Table 7
Stitching performance of proposed method.

Angles			HoloEntropy
a	b	c	
10	Nil	nil	2558.3
10	10	Nil	1647.7
10	10	-10	1284.4
10	10	10	957.09
10	20	Nil	842.87
10	20	10	1785.8
10	30	Nil	860.92
20	Nil	Nil	1129.7
20	20	10	1255
30	Nil	Nil	2907.7
30	10	Nil	1647.7
30	10	10	1724.7
30	30	10	1167.7
40	Nil	Nil	1500.5

values over the existing methods with multiple noise variants. For the images to be stitched with 0.005 noise effect, the average VSGV value obtained by the proposed method is 727.37, while the VSGV values of Euclidean distance based stitching, Minkowski distance based stitching and pairwise Euclidean distance based stitching have achieved 30.65%, 4.8% and 32% lesser than the VSGV value of the proposed method, respectively. Similarly, for the image with an increase in the noise variation has a lesser effect on the stitched image than other methods. The same can be observed from the increased VSGV values of the proposed stitching over the other stitching methods.

4.5. Under real time environment

Fig. 5 demonstrates the stitching performance of multiple methods under typical conditions. In Fig. 5(a) and (b), the images acquired from the camera kept at different positions and also unknown relative distance between those specific camera positions. In other words, the image captured at an arbitrary position and the arbitrary relative distance between those camera positions. In addition, Fig. 5(c–f) refers to the panoramic images obtained from all the methods. The comparative evaluation specifying HSGV and VSGV values of the proposed and conventional stitching methods is shown in Table 6. The proposed method attained the maximum HSGV value of 480.38. The worst case performance of HSGV value, i.e., 162.98 is achieved by the renowned Minkowski based image stitching. The VSGV value of Minkowski distance based stitching reached the limit of 394.26, and the proposed attained 407.15. Hence, the proposed stitching secures the first rank among all the four methods that illustrate the quality maintained in the stitched images. Fig. 6 demonstrates the camera position at different angles. Table 7 summarizes the stitching performance of the proposed method for different angles. Table 8 states the computational time complexity of the proposed and conventional methods.

Table 8
Computational complexity of the proposed and conventional methods.

Similarity Measures	Time (s)
Euclidean	18.5
Minkowski	15.6
Pairwise Euclidean	19.5
ASIFT (Morel and Guoshen, 2009)	25.8
FAST (Rosten et al., 2010)	22.5
FREAK (Alahi et al., 2012)	17.4
Chaos-inspired (Song et al., 2015)	18.4
Holoentropy	14.3

5. Conclusions

This paper presented a seamless image stitching scheme which performs well under varying illumination conditions. The proposed stitching scheme is based on holoentropy aided SIFT feature matching, which overcomes stitching problem concerned with scale, rotation and zooming effects of the images taken for stitching. The RANSAC image matching criteria is used in the proposed system to choose the inliers and the outliers representing the dominant frames with the significant visual content. The experimentation results of the proposed system are compared with the renowned Euclidean distance based stitching, which is the traditional image stitching method, Minkowski distance based image stitching and Pairwise distance based stitching. The performance is computed using the horizontal and vertical square gradient values. The experimental results indicate that the proposed image stitching scheme can handle images with noise and varying lighting conditions, with reduced misalignment and improved resolution.

References

Alahi, A., Ortiz, R., Vandergheynst, P., 2012. FREAK: Fast retina keypoint, IEEE Conference on Computer Vision and Pattern Recognition, Providence, RI, pp. 510–517.

Boykov, Y., Kolmogorov, V., 2004. An experimental comparison of mincut/max-flow algorithms for energy minimization in vision. IEEE Trans. Pattern Anal. Mach. Intell. 26 (9), 1124–1137.

Brown, M., Szeliski, R., Winder, S., 2005. Multi-image matching using multi-scale oriented patches. In: Proceedings of IEEE Computer Society Conference on Computer Vision and Pattern Recognition, vol. 1, pp. 510–517.

Brown, M., Lowe, D.G., 2007. Automatic panoramic image stitching using invariant features. Int. J. Comput. Vis. 74 (1), 59–73.

Candocia, F.M., 2003. Jointly registering images in domain and range by piecewise linear comparametric analysis. IEEE Trans. Image Process. 12 (4), 409–419.

Fang, X., Luo, B., Zhao, H., Tang, J., Zhai, S., 2010. New multi-resolution image stitching with local and global alignment. IET Comput. Vision 4 (4), 231–246.

Ganesa Moorthy, N., Nandhini Devi, S., 2014. Outlier detection through unsupervised approach with holoentropy. Int. J. Emerg. Technol. Comp. Sci. Electron. 7 (1), 154–158.

Hua, Zhen, Li, Yewei, Li, Jinjiang, 2010., Image stitch algorithm based on SIFT and MVSC, In: 2010 Seventh In proceedings of IEEE International Conference on Fuzzy Systems and Knowledge Discovery (FSKD), vol. 6, pp. 2628–2632.

Please cite this article in press as: Ane Delphin, D., et al. Holoentropy measures for image stitching of scenes acquired under CAMERA unknown or arbitrary positions. Journal of King Saud University – Computer and Information Sciences (2018), https://doi.org/10.1016/j.jksuci.2018.08.006

Huang, C.M., Lin, S.W., Chen, J.H., 2015. Efficient image stitching of continuous image sequence with image and seam selections. IEEE Sens. J. 15 (10), 5910–5918.

Kybic, J., 2004. High-dimensional mutual information estimation for image registration using control point and intensity. IEEE Trans. Image 13 (8), 1115–1127.

Lei, Z., Liu, X., Zhao, L., Chen, L., Li, Q., Yuan, T., Lu, W., 2016. A novel 3D stitching method for WLI based large range surface topography measurement. Optics Commun. 359, 435–447.

Li, Y., Wang, Y., Huang, W., Zhang, Z., 2008. Automatic image stitching using sift. In: proceedings of IEEE International Conference on Audio, Language and Image Processing, pp. 568–571.

Li, W., Jin, C.B., Liu, M., Kim, H., Cui, X., 2018. Local similarity refinement of shape-preserved warping for parallax-tolerant image stitching. IET Image Process. 12 (5), 661–668.

Li, J., Xu, W., Zhang, J., Zhang, M., Wang, Z., Li, X., 2015. Efficient Video Stitching Based on Fast Structure Deformation. IEEE Trans. Cybern. 45 (12), 2707–2719.

Li, J., Wang, Z., Lai, S., Zhai, Y., Zhang, M., 2018. Parallax-tolerant image stitching based on robust elastic warping. IEEE Trans. Multimedia 20 (7), 1672–1687.

Li, N., Xu, Y., Wang, C., 2018. Quasi-homography warps in image stitching. IEEE Trans. Multimedia 20 (6), 1365–1375.

Liu, R., Li, Z., Jia, J., 2008. Image partial blur detection and classification. In: Proc. IEEE Conf. Comput. Vis. Pattern Recognit. (CVPR), pp. 1–8.

Lowe, David G., 2004. Distinctive Image features from Scale Invariant Keypoints. J. Comp. Vision 60 (2), 91–110.

Lu, Y., Hua, Z., Gao, K., Xu, T., 2018. Multiperspective image stitching and regularization via hybrid structure warping. Comput. Sci. Eng. 20 (2), 10–23.

Ma, X., Liu, D., Zhang, J., Xin, J., 2015. A fast affine-invariant features for image stitching under large viewpoint changes. Neurocomputing 151 (3), 1430–1438.

Mills, A., Dudek, G., 2009. Image stitching with dynamic elements. Image Vis. Comput. 27 (10), 1593–1602.

Morel, Jean-Michel, Guoshen, Yu, 2009. ASIFT: a new framework for fully affine invariant image comparison. SIAM J. Imaging Sci. 2 (2), 438–469.

Peleg, S., 1981. Elimination of seams from photomosaics. Comput. Graph. Image Process. 16 (1), 90–94.

Rosten, E., Porter, R., Drummond, T., 2010. Faster and better: a machine learning approach to corner detection. IEEE Trans. Pattern Anal. Mach. Intell. 32 (1), 105–119.

Shu, Wu., Wang, Shengrui, 2013. Information-Theoretic outlier detection for large-scale categorical data. IEEE Trans. Knowl. Data Eng. 25 (3), 589–602.

Song, T., Jeon, C., Ko, H., 2015. Image stitching using chaos-inspired dissimilarity measure. Electron. Lett. 51 (3), 232–234.

Summa, B., Tierny, J., Pascucci, V., 2012. Panorama weaving: fast and flexible seam processing. ACM Trans. Graph. (TOG) 31 (4), 83.

Yang, Z.L., Guo, B.L., 2008. Image mosaic based on SIFT. In: Proceedings of IEEE International Conference on Intelligent Information Hiding and Multimedia Signal Processing, pp. 1422–1425.

Yang, X.H., Wang, M., 2013. Seamless image stitching method based on ASIFT. Comput. Eng. 39 (2), 241–244.

Zaragoza, J., Chin, T.J., Tran, Q.H., Brown, M.S., Suter, D., 2014. As-projective-as-possible image stitching with moving DLT. IEEE Trans. Pattern Anal. Mach. Intell. 36 (7), 1285–1298.

Zhi, Q., Cooperstock, J.R., 2012. Toward dynamic image mosaic generation with robustness to parallax. IEEE Trans. Image Process. 21 (1), 366–378.

Zitova, B., Flusser, J., 2003. Image registration methods: a survey. Image Vis. Comput. 21 (11), 977–1000.

Zoghlami, I., Faugeras, O., Deriche, R., Using geometric corners to build a 2D stitching from a set of images. In: Proceedings of the IEEE Computer Society Conference on Computer Vision and Pattern Recognition (CVPR), SanJuan, Puerto Rico,1997, pp. 420–425.

Please cite this article in press as: Ane Delphin, D., et al. Holoentropy measures for image stitching of scenes acquired under CAMERA unknown or arbitrary positions. Journal of King Saud University – Computer and Information Sciences (2018), https://doi.org/10.1016/j.jksuci.2018.08.006